Inorganic Chemistry Communications 135 (2022) 109088

Contents lists available at ScienceDirect

Inorganic Chemistry Communications

journal homepage: www.elsevier.com/locate/inoche

Short communication

The effect of *thymus syriacus* plant extract on the main physical and antibacterial activities of ZnO nanoparticles synthesized by SILAR method

B. Şahin [a,*], R. Aydin [b], S. Soylu [c], M. Türkmen [d], M. Kara [c], A. Akkaya [e], H. Çetin [f], E. Ayyıldız [g]

[a] Laboratory of Nanostructured Materials and Applications, Faculty of Arts and Sciences, Hatay Mustafa Kemal University, Hatay, Turkey
[b] Department of Physics, Faculty of Sciences, Selcuk University, Konya, Turkey
[c] Department of Plant Protection, Faculty of Agriculture, Hatay Mustafa Kemal University, Hatay, Turkey
[d] Department of Field Crops, Faculty of Agriculture, Hatay Mustafa Kemal University, Hatay, Turkey
[e] Mucur Technical Vocational Schools, Tech.Prog. Department, Ahi Evran University, Kırşehir, Turkey
[f] Department of Physics, Faculty of Arts and Sciences, Yozgat Bozok University, Yozgat, Turkey
[g] Energy Conversion Research and Application Center, Department of Physics, Faculty of Sciences, Erciyes University, Kayseri, Turkey

ARTICLE INFO

Keywords:
Green synthesis
ZnO
Thymus syriacus
Antibacterial activity

ABSTRACT

This study aimed to determine the main physical properties of green synthesized ZnO nanoparticles (ZnO-NPs) using *Thymus syriacus* plant extract and their antibacterial activities against eight different Gram-positive and Gram-negative plant bacterial disease agents. The surface morphological, structural, optical and electrical attributes of the ZnO films were analyzed by various types of characterization techniques. The authors have observed that the microstructural and surface morphological properties considerably changed by using *T. syriacus* plant extract. UV–Vis. analysis showed that the bandgap values are increased from 3.17 to 3.28 eV with the *T. syriacus* content in the growth solution. Impedance measurements presented an increase of the semicircle diameters with the increase % *of T. syriacus*. The antibacterial effectiveness of ZnO-NPs was evaluated against plant pathogenic bacterial species by using the agar disc diffusion method. Established on inhibition zone diameter values, ZnO-NPs displayed varying levels of antibacterial activities against all bacterial species tested. Gram-positive bacterial species were found more sensitive than Gram-negative species. In comparison, the highest antibacterial activity was displayed against *Clavibacter michiganensis* subsp. *michiganensis* and *Bacillus subtilis* subsp. *subtilis*, the lowest antibacterial activity was recorded for *Pseudomonas corrugata*. The present research findings suggest that the green synthesized ZnO-NPs have a prospective to be used as optoelectronic materials and antibacterial agents against plant pathogenic bacterial disease.

1. Introduction

Lately, nanostructured metal oxide particles including MgO, CuO, TiO_2, and ZnO have augmented the relevance to be used in many technological applications [1-4]. Among these different kinds of nanoparticles, zinc oxide (ZnO) is an ample, innocuous and low cost oxide material with high mechanical and chemical stability. ZnO is also an II–VI wide bandgap transition metal oxide with enormous exciton binding energy (60 meV) and n-type semiconductor with direct energy band gap of ≈3.2 eV at room temperature. ZnO has attracted great attention because of its impressive biological, chemical, and physical characteristics [5-8].

Nowadays, ZnO nanoparticles (ZnO-NPs) were used extensively in many applications such as the pharmaceutical industry, smart UV sensors, dye-sensitized solar cells, biosensors, drug delivery, photocatalysts, light-emitting devices, antioxidant activity, and gas sensors [9-14]. ZnO-NPs have been obtained through many procedures, including spray pyrolysis, chemical precipitation, micro-emulsion, sol–gel, chemical vapor deposition, electrodeposition microwave radiation, hydrothermal and successive ionic layer adsorption and reaction (SILAR), etc [15-19]. Although there are some different ways to synthesize ZnO nanomaterials, the SILAR procedure is widely used, for it is relatively cost-effective, easy, and low temperature [20-22].

Green synthesis involves synthesis through algae, bacteria, fungi, and plants, etc. The use of plants for the deposition of NPs is a low-priced, rapid and eco-friendly option and is innocuous for human use. Besides, the synthesis by plant extracts is beneficial because it decreases the risk of further contamination by reducing the reaction time and

* Corresponding author.
E-mail address: bsahin@mku.edu.tr (B. Şahin).

https://doi.org/10.1016/j.inoche.2021.109088
Received 13 September 2021; Received in revised form 16 November 2021; Accepted 23 November 2021
Available online 25 November 2021

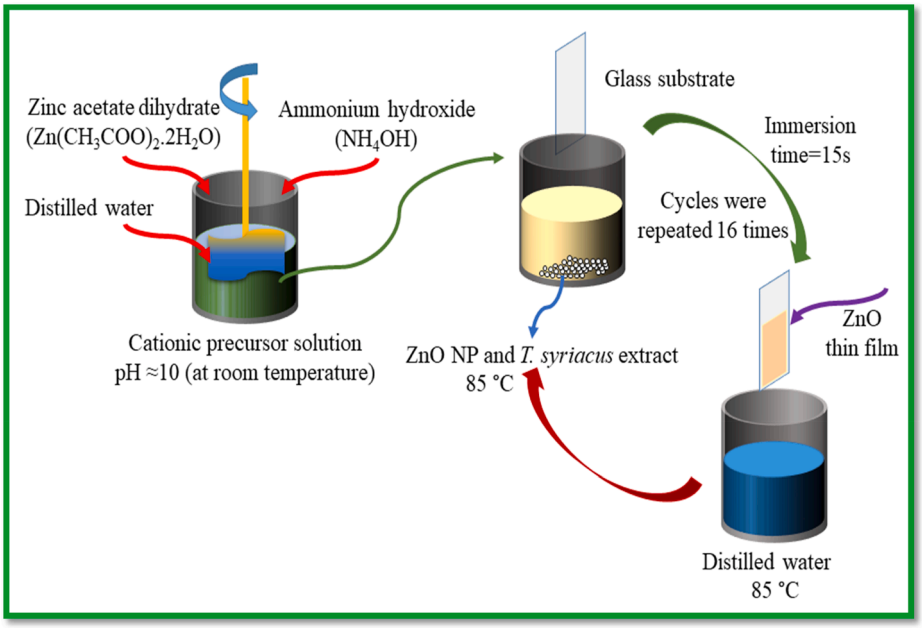

Fig. 1. The scheme of SILAR method for the growth of nanostructured ZnO samples.

preserving the cell structure. Various investigations have been conducted on the green synthesis of several nanostructured metal oxides using extracts from certain plant species as a biological origin [23-27]. ZnO-NPs are favored over other nanostructured metal oxides hence their superior antibacterial potential and bio-compatible natures [13,27]. The primary contraption of the bactericidal nature of ZnO-NPs includes physical linkage between the bacterial cell wall and ZnO-NPs, generation of free radicals, reactive oxygen species (ROS). Releases of Zn^{2+} ions also display antibacterial activities that are useful for the biological and pharmaceutical practices [28].

Plant diseases caused by particular plant bacterial species are major limitations and cause enormous yield losses in agriculture globally. Depending on the infection stage and environmental conditions, annual yield loss caused by specific bacterial pathogens could reach up to 5–50% [29]. Currently, the management of bacterial diseases is mainly achieved by cultural (such as the use of clean certified seeds) or chemical treatment (such as applying chemical pesticides and antibiotics). Although the application of cultural and chemical control measures may control disease occurrence, the effectiveness of these methods for controlling bacterial diseases is usually limited. Because of the several adverse side effects, such as high cost, development of pesticides/antibiotic-resistant isolates, residues on crops, governmental restriction, and the public interest of environmental consideration, several types of research were intensified to utilize novel environmentally friendly control measures against bacterial disease [30]. Nowadays, researchers have focused on the synthesis of different nanoparticles using various synthesis routes of plant and animal origin [31]. The genus *Thymus,* belonging to the Lamiaceae plant family, contains over 300 evergreen species that are naturally grown in Southern Europe and Asia. *Thymus syriacus* Boiss, known as thyme, is native plant species and can be found growing wildly in the eastern Mediterranean region [32]. The chemical composition and high-level antimicrobial activity of essential oil and major constituents of *T. syriacus* have been assessed against gram-negative human pathogenic bacterial species [33]. Although a limited number of studies are available on antibacterial performances of nanostructured green synthesized particles against fungal and bacterial disease agents [34-36], to the best of our knowledge, the antimicrobial activities of green synthesized ZnO-NPs using *T. syriacus* aqueous leaf extract against plant bacterial disease agents have never been tested before.

Hence, multiple aims of the present study were to analyze green synthesized (using *T. syriacus* leaf extract) nanostructured ZnO films by using novel characterization methods. Besides, the antibacterial potentials of two different concentrations of ZnO-NPs were also evaluated *in vitro* against Gram-positive and Gram-negative bacterial disease agents such as *Bacillus subtilis* subsp. *subtilis, Clavibacter michiganensis* subsp. *michiganensis*, *Pseudomonas syringae* pv. *phaseolicola*, *P. syringae pv. syringae, P. cichorii, P. corrugate, Pectobacterium carotovorum* subsp. *carotovorum* and *Xanthomonas axonopodis* pv. *juglandis*.

2. Material and methods

2.1. Plant material and preparation of plant extract

Wild populations of *T. syriacus*, used in the preparation of ZnO-NPs, were collected from the naturally growing sites of wild populations of *T. syriacus* in Hatay Province located in the Eastern Mediterranean Region of Turkey (36°21′24″N 36°10′32″ E). Plant species was further identified by Prof. Dr. I. Uremis and voucher specimen of the plant has been deposited in the herbarium of the BISAK unit of Hatay Mustafa Kemal University (No. TsyAl25). Dried leaves of *T. syriacus,* which were used for extraction, were washed with distilled water and ground in a plant mill. The aqueous leaf extract of *T. syriacus* was prepared by boiling dried powdered plant leaves (10 g) in double-distilled water (100 mL) for 15 min, cooled down to room temperature, and finally filtered using Whatman filter paper (No.1). The aqueous filtered plant extract was stored in a fridge at 4 °C to synthesize ZnO-NPs as previously described [36].

2.2. Green synthesis of ZnO-NPs

ZnO films with and without *T. syriacus* were obtained onto glass substrates by the SILAR procedure. *T. syriacus* as a plant extract was used in the deposition process to change ZnO films' nanostructures. All the chemicals, including zinc acetate dihydrate ($Zn(CH_3COO)_2{\cdot}2H_2O$), acetone ($(CH_3)_2CO$), and ammonium hydroxide (NH_4OH) were of analytical reagent quality and were used without any further purification.

To obtain the cationic precursor solution, 2.2 g zinc acetate dihydrate was blended with 100 mL double-distilled water, which resulted in

0.1 M zinc acetate solution. Ammonium hydroxide (NH_4OH) was supplemented to the cationic solution to regulate the value of pH ≈ 10. NH_4OH was added to the growth bath drop by drop under constant stirring until the pH values reached about 10. The cationic aqueous solution was maintained at a temperature of 85 °C. The glass slides were immersed in the solution bath for 15 s. Then to dismantle the unreacted ions on the surface of the glass substrate, the substrate was rinsed with double distilled water 15 s. This SILAR cycle was applied 16 times to acquire adherent and uniform ZnO films. Likewise, to investigate the impression of the *T. syriacus* content to the ZnO films *T. syriacus* extract was supplemented to each precursor solution, and two series of specimens were deposited. Fig. 1. shows the solution-based SILAR method's scheme for the deposition of ZnO films and particles. Eventually, the obtained ZnO films and powders with and without *T. syriacus* were heated at 525 K for 30 min.

2.3. Characterizations of ZnO-NPs

The SILAR synthesized ZnO films were analyzed using varied techniques. Crystallographic attributes were carried out using Bruker D8 Advance, a high-resolution X-ray diffractometer (XRD) with CuK_α radiation ($\lambda = 1.540056$ Å). The surface topography measurements of the grown films were studied by Scanning Electron Microscope (SEM, Jeol JEM-2100F) and Atomic Force Microscope (AFM, Solaris Atomic Force Microscope). The elemental composition in the prepared ZnO film was confirmed by using energy-dispersive X-ray spectroscopy (EDX) attached to SEM. The thickness of the films was acquired using a surface profilometer (Nanomap – 500LS 3D). The existence of chemical bonding in green synthesized ZnO films was studied by Thermo Scientific Nicolet 6700 FTIR spectrometer. UV–visible absorption and transmittance spectra of the green synthesized ZnO films were determined with a UV–Vis. spectrometer (Thermo Scientific Genesys 10S UV–Vis.) between 190 and 1100 nm at room temperature. Impedance measurements were performed on films and an HP 4284 A LCR meter, which has a measurement frequency range of 20 Hz-1 MHz. All the impedance measurements were performed at room temperature.

2.4. Bacterial microorganisms and preparation of inoculum suspension

Bacterial cultures of *C. michiganensis* subsp. *michiganensis* (*Cmm*Ad12), *B. subtilis* subsp. *subtilis* (*Bss*A19), *P. cichori* (*Pc*Sa2), *P. syringae* pv. *phaseolicola* (*Psp*E22), *Pectobacterium carotovorum* subsp. *carotovorum* (*Pcc*Sy17), *P. corrugata* (*Pc*Sa27), *P. syringae* pv. *syringae* (*Pss*E8) and *X. arboricola* pv. *juglandis* (*Xaj*E5) used in the study were isolated from their host plants such as tomato, lettuce, bean, potato, citrus, and walnut. Identities of bacterial isolates used in this study were confirmed by using MALDI-TOF and molecular analyses [37]. Bacterial isolates were stored on Trypic Soybean Agar (Merck, Darmstadt, Germany) medium at 4 °C until further tests.

Bacterial suspensions were prepared from a single colony of stock culture and inoculated in a commercial Luria Broth (Merck, Darmstadt, Germany) liquid growth medium. The resulting bacterial culture was incubated at 26 °C on an orbital shaker for 24 h to grow a sufficient population. Bacterial suspensions were subsequently prepared in sterile 10 mM $MgCl_2$ solution, and their concentrations were adjusted to 10^8 cfu ml^{-1} spectrophotometrically ($OD_{\lambda 620} = 0.15$) as described earlier [38].

2.5. Antibacterial application test of ZnO-NPs

The stock solution of green synthesized ZnO-NPs was prepared by dissolving 500 mg ZnO-NPs in 1 mL sterile dimethyl sulfoxide (DMSO, Merck, Darmstadt, Germany).

The agar disc diffusion method was used for the determination of the qualitative antibacterial assay of the ZnO-NPs. The obtained bacterial suspensions (250 μL at 10^8 cfu ml^{-1} concentration) were uniformly spread over petri plates containing Trypic Soybean Agar medium and sterile 5 mm diameter discs (Antibiotic susceptibility test discs, Bioanalyse, Turkey). They were treated with 10 μL/disc of the ZnO-NPs, and gently pressed onto nutrient media to ensure contact with the surface of the media. The inoculated petri plates with bacterial isolates were left 30 min at room temperature to allow the diffusion of the tested ZnO-NPs, sealed with sterile parafilm, and then were incubated at 26 °C for 48 hr. At the end of the period, a clear zone of inhibition (expressed as mm) around the disc was measured for the antibacterial activity of ZnO-NPs by using a steel ruler. Negative control was prepared using sterile DMSO employed to prepare ZnO-NPs.

In vitro antibacterial studies were performed in three different petri plates for each treatment. The obtained data were analyzed using variance analysis (ANOVA) using the SPSS Statistic program (Version 17.0). Significant differences between treatments were compared using Duncan's Multiple Range Test ($P \leq 0.05$).

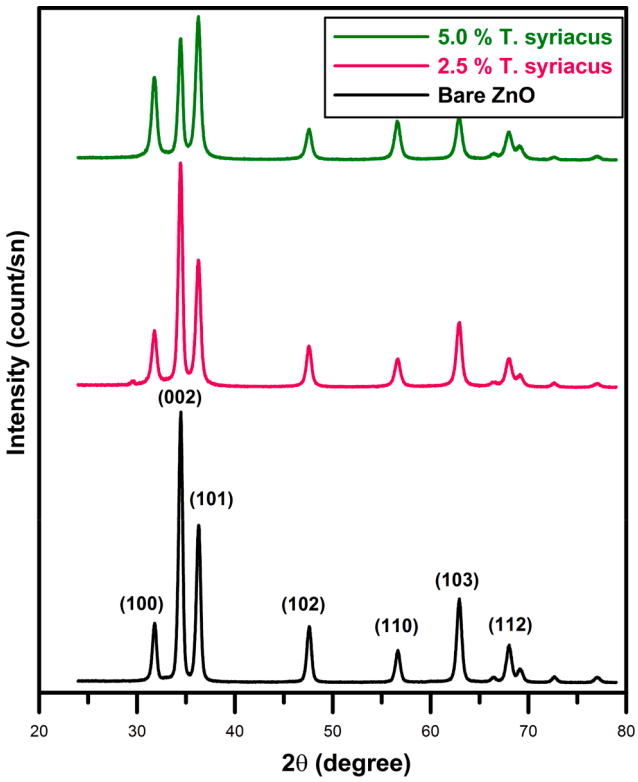

Fig. 2. XRD patterns of SILAR derived ZnO films synthesized without (bare ZnO) and with *T. syriacus* plant extract.

3. Results and discussions

3.1. Structural analysis of ZnO-NPs

Structural properties all produced ZnO films examined by using X-

Table 1
Relative peak intensity, crystallite size and film thicknesses of green synthesized ZnO-NPs.

Sample	Relative Peak Intensity (cps) (002)	Crystallite Size (nm)	Film Thickness (μm)
Bare ZnO	16,423	17.19	1.82
2.5 % *T. syriacus*	13,910	15.62	1.74
5.0 % *T. syriacus*	7291	14.51	1.40

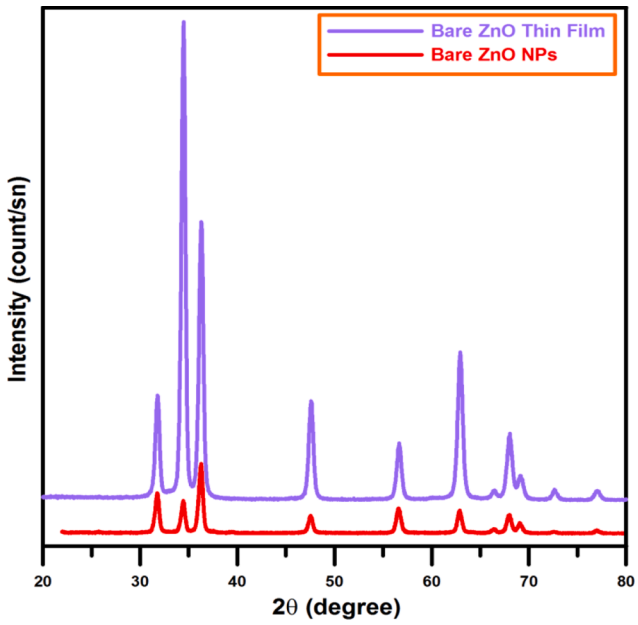

Fig. 3. XRD patterns of SILAR derived ZnO thin film and NPs synthesized without *T. syriacus* plant extract.

ray diffraction analyses. The crystallite size values were calculated by using the XRD data. Fig. 2. indicates the XRD patterns of ZnO films with and without leaf extract *T. syriacus* on glass substrates. From the patterns, it is obvious that all ZnO films are grown preferentially on (0 0 2) and (1 0 1) planes. Except for those two basic peaks, there are five more diffraction lines of (1 0 0), (1 0 2), (1 1 0), (1 0 3), and (1 1 2) planes. These observed XRD results are exactly similar to the results of previous studies [39,40]. The planes are indexed to polycrystalline ZnO phase nature with a hexagonal wurtzite structure (JCPDS file No. 0 01–075-6445) [41]. The relative intensity of the (0 0 2) peak was presented in Table 1.

Table 1 shows that the peak intensities decreased by adding *T. syriacus* extract to the aqueous solution [42,43]. Fig. 3. shows XRD patterns of SILAR derived ZnO thin film and powders synthesized without *T. syriacus* plant extract. It can be seen that the relative peak intensities of ZnO powders are smaller than thin-film structures.

To find the *T. syriacus* effect on the structural parameters, the crystallite size (D) values of the *ZnO-NPs* are estimated from their XRD patterns via the well-known Scherrer equation [44]:

$$D = \frac{K\lambda}{\beta cos\theta} \quad (1)$$

where K, λ, β, *and* θ are the Scherrer's constant, the X-ray wavelength, the FWHM value of the peak and θ the Bragg's angle of the peaks, respectively. Estimated crystallite size values are given in Table 1. The average crystallite size of ZnO film is decreased by *T. syriacus* from 17.19 to 14.51 nm, which means the addition of *T. syriacus* to the precursor solution, alters the crystallite growth. A similar trend of crystallite size was reported by [45,46]. For the solution-based metal oxide growth process, the formation of nanostructured materials is vigorously related to the chemical composition of the growth bath. The plant extracts as reducing agent and stabilizers of NPs like T. sysriacus are the significant agents that can efficiently reduce speed and with this the crystallinity quality and particle size. The existence of *T. syriacus* in the starting solution may further modify the diffusion percentage of Zn and O hence leading to the alteration of structure, size and morphology [47,48].

3.2. Surface morphological analysis of ZnO-NPs

It is quite essential to study the surface morphological properties of films because the surface shapes of the nanostructured ZnO films affect their optical application efficiency. Surface morphologies of synthesized ZnO films were investigated by SEM. The SEM pictures of the ZnO films with diverse concentrations of *T. syriacus* (0%, 2.5%, and 5.0%, respectively) grown on glass slides were demonstrated in Fig. 4. As can be seen from SEM images, all ZnO films exhibited a homogeneous and dense surface structure. The addition of plant extracts in the deposition

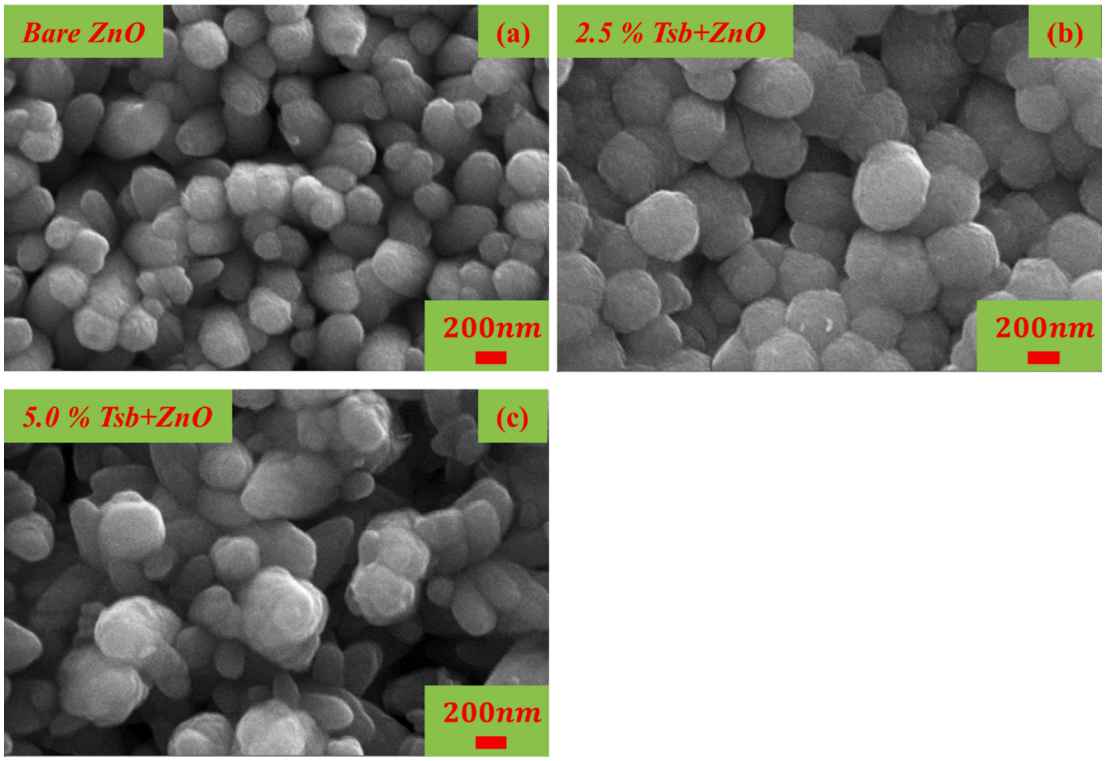

Fig. 4. SEM micrographs of SILAR derived ZnO films synthesized without (bare ZnO) and with *T. syriacus* plant extract.

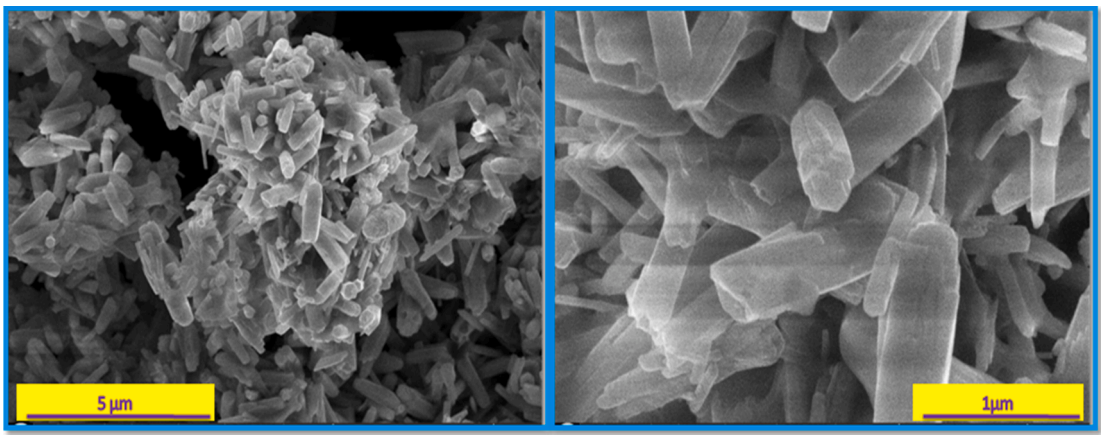

Fig. 5. SEM micrographs of SILAR derived ZnO-NPs synthesized without *T. syriacus* plant extract.

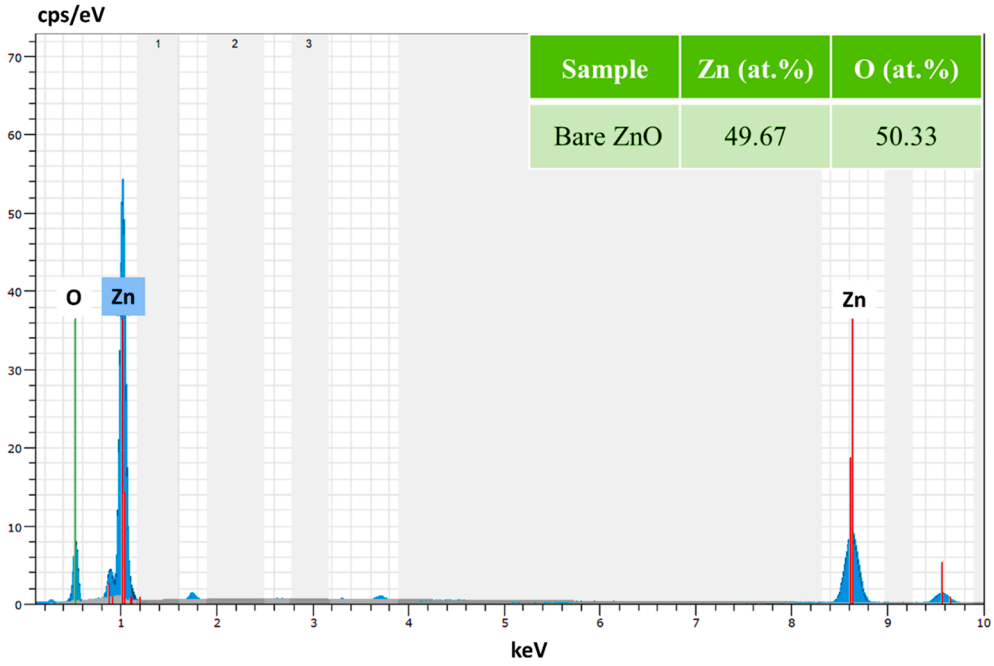

Fig. 6. EDX spectrum of SILAR derived bare ZnO film.

bath is exceedingly crucial for nanostructured metal oxide films and powders. Because it displays an important mission in arranging their surface morphological, optical, and electrical properties.

The bare ZnO film has rod-shaped particles as denoted in Fig. 4 (a). We observed that the *T. syriacus* plant extract content in the bath solution impresses the ZnO samples' particle morphology and crystalline quality. As illustrated by the SEM images, with increasing *T. syriacus* plant extract concentration, the prepared ZnO samples displayed a homogeneous and dense surface structure with changing size. From Fig. 4 (b,c) it is seen that when *T. syriacus* is added into the reaction mixture, ZnO films exhibit densely packed, nearly spherical-like ZnO crystals [49,50]. That is to say, the leaf extract *T. syriacus* plays a major role in the formation of surface morphology of ZnO film [11,51,52]. The variation in plant extract content of the bath solution depicted different sizes and morphologies of ZnO Nps and films. Hence, the *T. syriacus* plant extract can be used as a modifier and stabilizer agent to alter the morphology and crystalline quality of metaloxide-based samples. Also, Fig. 5. displays the SEM micrographs of SILAR derived ZnO powders synthesized without *T. syriacus* plant extract.

The chemical elemental analysis of bare ZnO film is defined by energy-dispersive X-ray spectroscopy (EDX). The EDX spectrum for ZnO film is depicted in Fig. 6. The sharp peaks in the spectrum verify the presence of Zn and O elements. The atomic percentages of Zn and O in the film are measured as 49.67 and 50.33 %, respectively.

3.3. AFM analysis of ZnO-NPs

The condition of the surface of ZnO films synthesized without and with *T. syriacus* plays a crucial role in determining not only electrical properties but also some physical properties such as the film nature and the functional performance. Fig. 7. illustrates AFM topography photos with a 10x10 μm^2 scan size of the three examined film surfaces. Micrographs showed that films are tightly packed and granular; any sign of aggregation of grains almost does not exist. It can be seen in Fig. 7. the microstructure varies with the adding of *T. syriacus* in growth solution, the grains have less sharp edges, and for the first sight it seems that the surface is rough and grains are much bigger.

Surface structure parameters Sa (Average surface roughness), Sq (Root mean square), and Sz (Ten-point height) are listed in Table 2. According to Table 2, as can be seen in SEM images and XRD spectra,

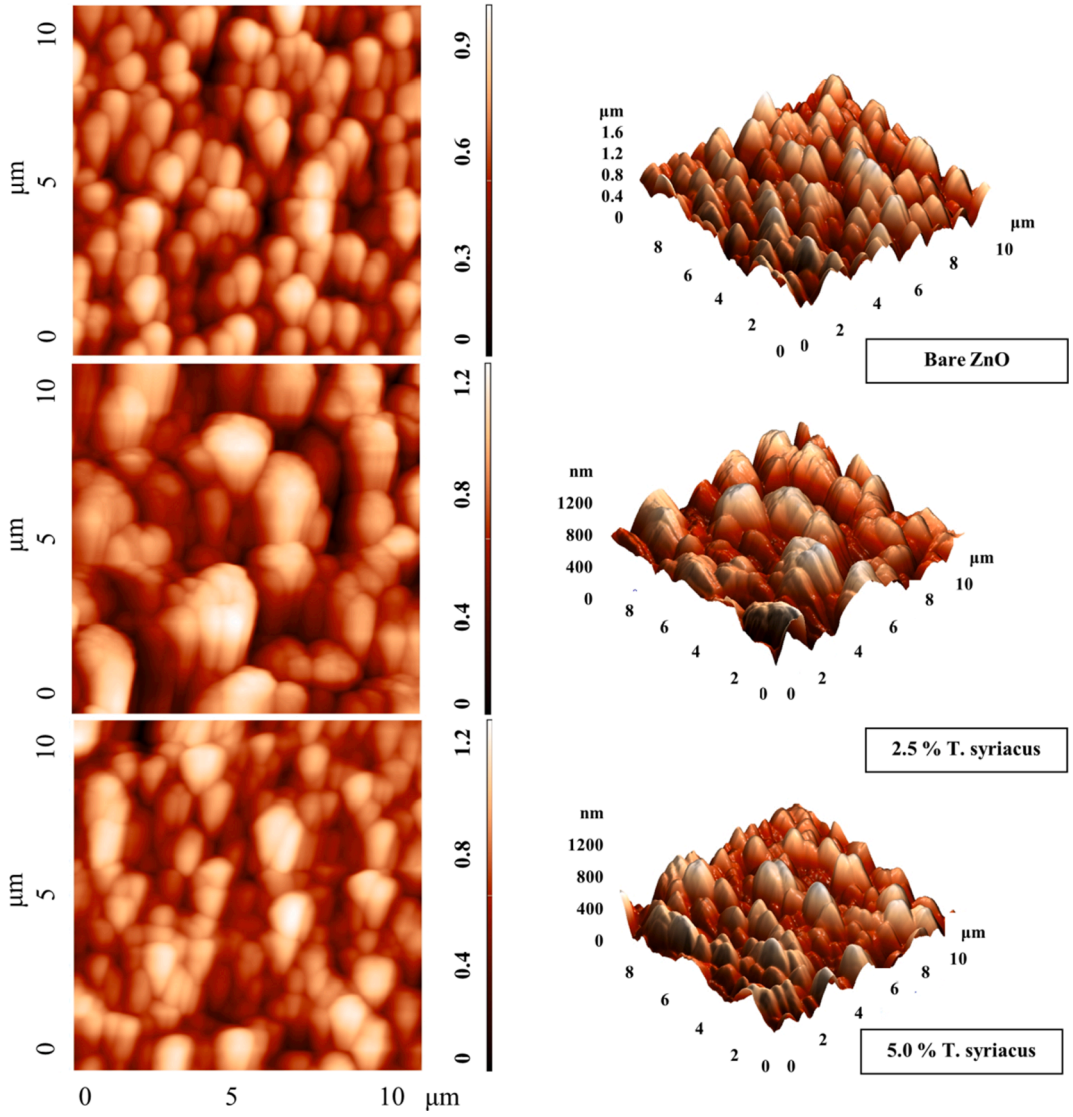

Fig. 7. AFM images of SILAR derived ZnO films synthesized without (bare ZnO) and with *T. syriacus* plant extract.

Table 2
Surface roughness parameter and band gap energy values of ZnO films synthesized without and with *T. syriacus*

Sample	Sa (nm)	Sz (nm)	Sq (nm)	Bandgap(eV)
Bare ZnO	122	494	152	3.17
2.5 % *T. syriacus*	183	621	221	3.21
5.0 % *T. syriacus*	161	652	199	3.28

particle size changed significantly after adding *T. syriacus* in the growth solution, so the Sa, Sq, and Sz values also changed. These findings are in excellent concurrence with the results of the SEM investigations.

3.4. FTIR analysis of ZnO-NPs

FTIR spectroscopy is an advantageous technique for investigating vibrational modes of synthesized materials. This method was used to investigate various vibration modes of synthesized ZnO films. The FTIR spectrum of films is shown in Fig. 8. In general, metal-oxides show an absorption band below 1000 cm^{-1}), which arises from inter-atomic vibrations. Peaks appearing at ~ 853 cm^{-1}, 728 cm^{-1}, and ~ 560 cm^{-1} can be assigned to the ZnO characteristic stretching modes [57,58]. However, the peak at the 1583 cm-1 range belongs to the stretching

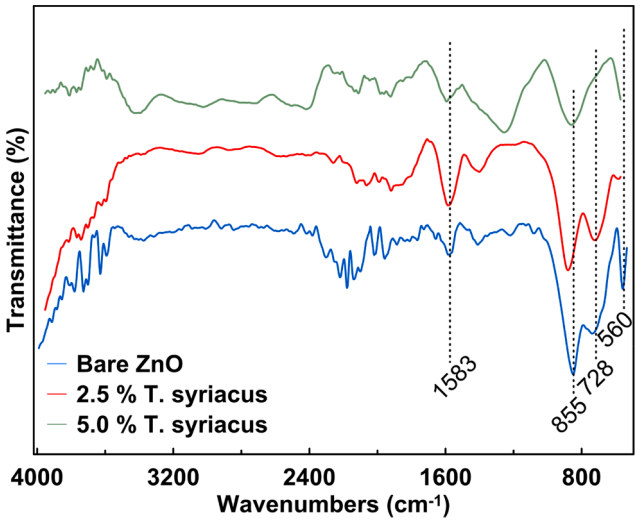

Fig. 8. FTIR spectroscopy of SILAR derived ZnO films synthesized without (bare ZnO) and with *T. syriacus* plant extract.

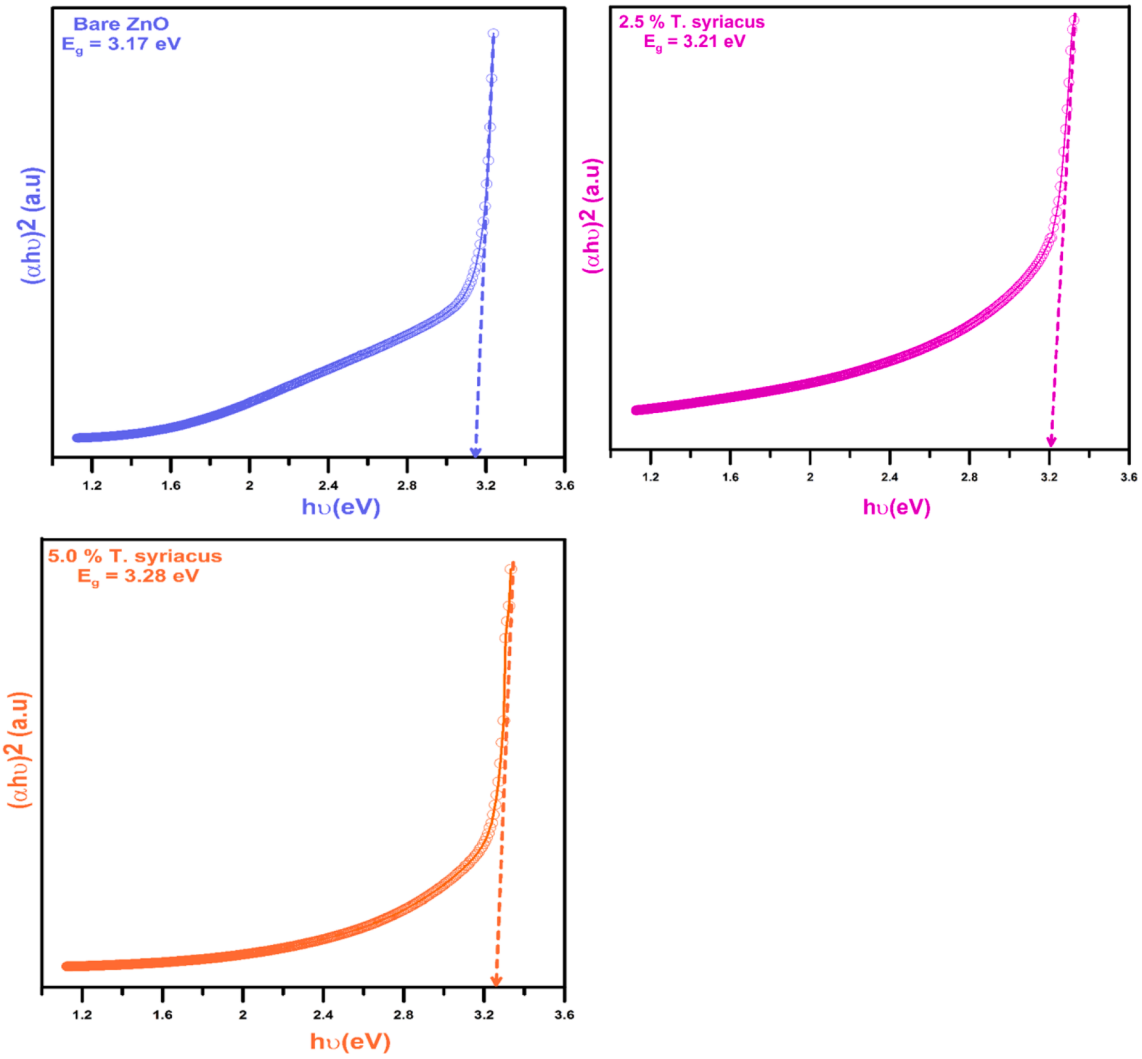

Fig. 9. Plots of $(\alpha h\upsilon)^2$ versus $(h\upsilon)$ of SILAR derived ZnO films synthesized without (bare ZnO) and with *T. syriacus* plant extract.

vibration of the C = O group and indicates the presence of some acetate moieties at the surface [53].

The peaks of ZnO are compatible with the literature [53-55]. However, the peak of organic compounds occurs when *T. syriacus* is added to the growth solution. These peaks belong to a wide variety of compounds. Water-distilled oil from aerial parts of *T. syriacus* contains 34 (corresponds to 94.75% of the oil) components, and the main components are thymol, carvacrol, p-cymene, borneol, and γ-terpinene [56]. These monoterpenoid phenols and monoterpene derivatives (and other known 29 components of oil) did not create a sharp spectrum peak but a weak broad peak around the functional group region.

3.5. Optical analysis of ZnO-NPs

The optical bandgap (E_g) of the ZnO films without and with *T. syriacus* were estimated by Tauch's relation [57]:

$$\alpha h\nu = (h\nu - E_g)^n \quad (2)$$

where *n, E_g, α, and hν* are characterized which absorption process is involved in the sample (n = 1/2 for direct bandgap transitions), the optical bandgap energy, the absorption coefficient, and the photon energy, respectively. To analyze the effect of *T. syriacus* on the bandgap diagrams of ZnO films $(\alpha h\nu)^2$ versus $(h\nu)$ were drawn (Fig. 9) as a function of plant extract material. Using this graph, the E_g values were found to be 3.17, 3.21, and 3.28 eV for bare, 2.5 %, and 5.0 % *T. syriacus*

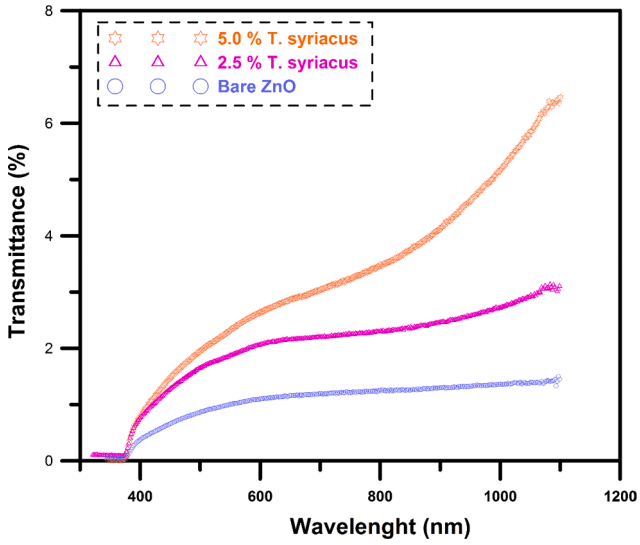

Fig. 10. Transmittance spectra of SILAR derived ZnO films synthesized without (bare ZnO) and with *T. syriacus* plant extract.

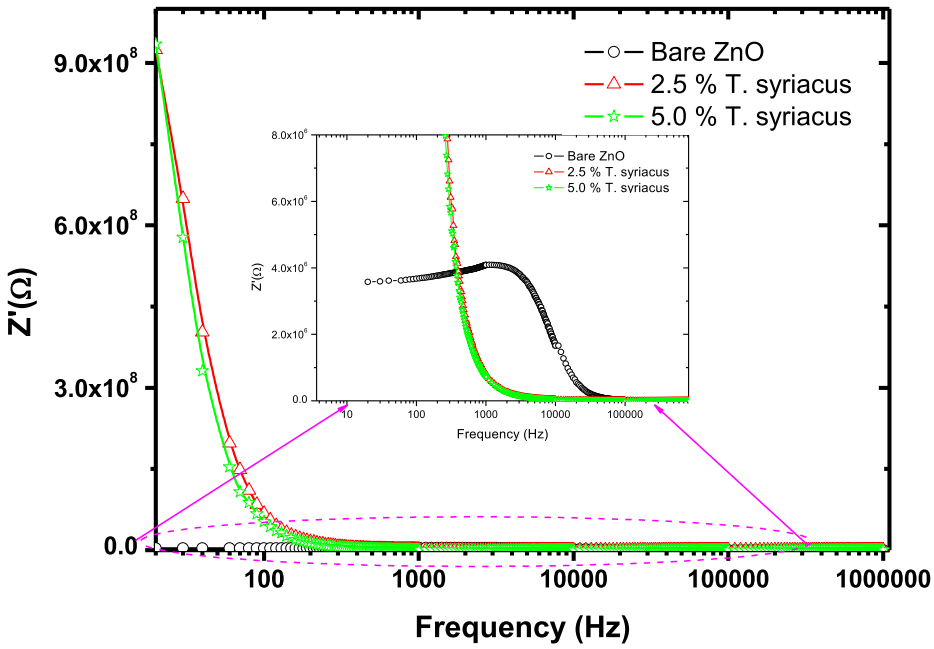

Fig. 11. Variation Z' with frequency of SILAR derived ZnO films synthesized without (bare ZnO) and with *T. syriacus* plant extract.

added ZnO films, respectively. These values are also summarized in Table 2. A parallel trend was also reported in the previous works [58,59]. It is clear from Fig. 9 that the bandgap value ascends by augmenting the *T. syriacus* concentration in the ZnO film. This variation of the bandgap energy may be attributed to the impression of several factors like structural parameters, film thickness, crystallite size, etc. [60-62]. As the supplementation of *T. syriacus* plant extract in the bath boosts the nucleation process which alters the crystallization quality hence modifying the optical properties. Furthermore, the presence of *T. syriacus* in the growth solution may additionally modify the diffusion proportion of Zn and O at the substrate and hereby lead to the variation of main physical properties.

The optical transmittance spectra of the ZnO films in the wavelength range of 200–1200 nm are depicted in Fig. 10. As it can be seen from Fig. 10. bare ZnO film has the lowest transmittance. The transmittance augmented with enhancing *T. syriacus* content in the aqueous solution bath. This alteration in transmittance can be imputed to adjusted crystallinity attributes, crystallite size, and film thickness [63,64].

3.6. Impedance analysis of ZnO-NPs

The impedance spectroscopy makes it possible to allocate the real (resistive) and the imaginary (reactive) part of the electrical characteristic of the materials to investigate an obvious picture of the sample characteristics. Fig. 11. shows changes of the real part of complex impedance with frequency for the bare ZnO, 2.5%, and 5.0 % *T. syriacus* samples. At the low-frequency region of the graph, a relatively higher Z' value is noticed due to the effectiveness of resistive grain boundaries for

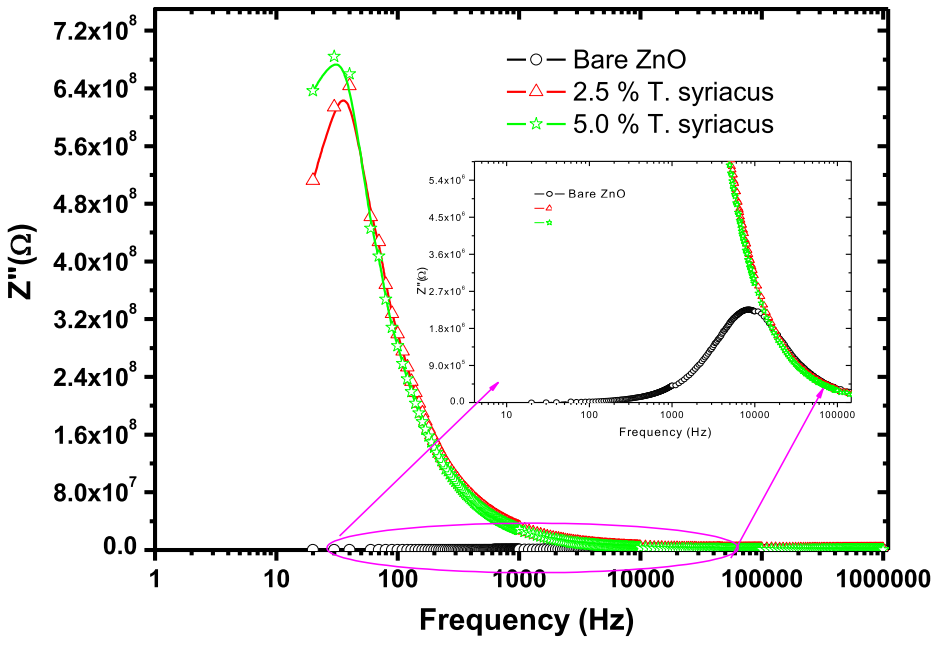

Fig. 12. Variation Z'' with frequency of SILAR derived ZnO films synthesized without (bare ZnO) and with *T. syriacus* plant extract.

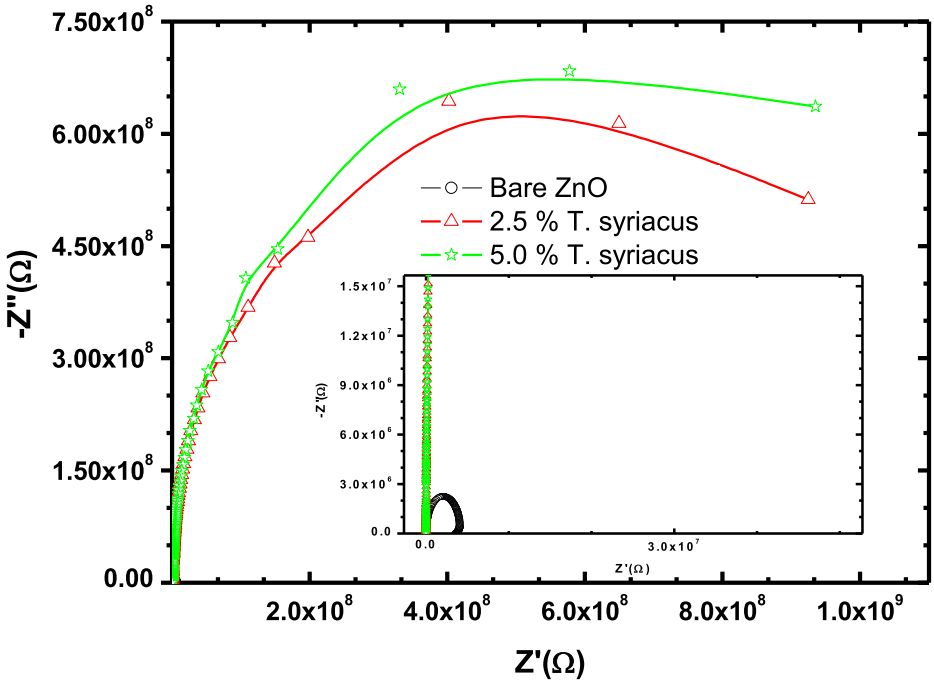

Fig. 13. Complex plane of the impedance for the bare ZnO and *T. syriacus* added samples, at room temperature.

all the samples [65,66]. Especially, 2.5% and 5.0 % *T. syriacus* samples have relatively higher Z' at the low-frequency region. The AFM results show that 2.5% and 5.0 % T. syriacus additives cause greater grains than the bare ZnO sample. *T. syriacus* content may create charge accumulation at grain boundaries. The grain boundary-space charge effect could cause higher impedance at the low-frequency region [67]. At the high-frequency region of the graph, a decrease for Z' all the samples appears, maybe due to increasing ac conductivity [68]. After the substantial variation in Z' in the low-frequency region is followed by saturation in the high-frequency region. The inset makes possible the visibility of the graph of the bare ZnO with relatively low Z' values. The graph for the bare ZnO has a maximum Z' value at a relatively higher frequency region, while those of the % *T. syriacus* addictive samples have peaks at the low frequency.

Fig. 12 indicates the variation of the imaginary part of the impedance with frequency. The graph gives us an insight into the electrical relaxation process. When the graph is viewed, a correlation between % *T. syriacus* addiction and the peak position of the graph at the frequency-axis is noticeable. The higher % *T. syriacus* addiction causes peak location at the lower frequency while the bare ZnO has a peak at the near of 10.000 Hz. The presence of the single peak in the bare ZnO is associated either with grain or grain boundary depending upon the respective resistance value. These results show the presence of different relaxational processes for all samples [69].

The Cole-Cole graph of all the samples is given in Fig. 13. The inset was again prepared for the bare ZnO sample. A slight decentralization of the semicircle can be associated with a relaxation time distribution. The fact of a single semi-circular arc confirms the presence of resistance due to the intrinsic grain boundary effect [70]. While the bare ZnO sample has a semicircle with the smallest radius, 2.5%, and 5.0 % *T. syriacus* samples have higher radiuses, which are related to grain boundary resistance.

3.7. Antibacterial activities of ZnO-NPs

The antibacterial activities of different concentrations (2.5% and 5.0%) of ZnO-NPs were investigated by standard disc diffusion technique (Fig. 14). The inhibition zones formed by ZnO-NPs against bacterial species tested were given in Table 3. Although low quantities were used, ZnO-NPs exhibited significantly varying levels of antibacterial activities against all bacterial species tested. In general, ZnO-NPs with *T. syriacus* extract caused significantly higher inhibition zones against tested bacterial isolates in comparison to pristine ZnO-NPs. In each case, ZnO-NPs displayed an increasing antibacterial activity as their concentration increased. Based on the inhibition zone diameter recorded, Gram-positive bacterial species were found to be more sensitive than Gram-negative species. The strongest antibacterial activities were observed against Gram-positive bacterial agents *C. michiganensis* subsp. *michiganensis* and *B. subtilis* subsp. *subtilis* followed by Gram-negative bacterial disease agents *P. syringae* pv. *phaseolicola*, *P. cichorii*, *P.syringae* pv. *syringae*, *X. axonopodis* pv. *juglandis*, *P. caratovorum* subsp. *carotovorum* and *P. corrugata*, respectively (Table 3). The mean observed inhibition zones ranged between 28.67 and 35.0 mm were recorded for Gram-positive *C. michiganensis* subsp. *michiganensis* and 14.67 and 20.33 mm for *B. subtilis* subsp. *subtilis*. Among the Gram-negative bacterial species, the highest antibacterial activity was recorded against *P. syringae* pv. *phaseolicola* with the mean zone of inhibition values of 11.0 and 19.33 mm, followed by *P. cichorii* (between 9.0 and 17.0 mm) *P. syringae* pv. *syringae* (between 7.67 and 14.0 mm), *X. axonopodis* pv. *juglandis* (between 8.0 and 13.33 mm), *P. caratovorum* subsp. *carotovorum* (between 6.33 and 12.33 mm) and *P. corrugata* (between 6.0 and 7.0 mm), respectively. Sterile DMSO, which was used as the negative control, did not cause inhibition zone against bacterial microorganisms tested (Fig. 14 I)

In recent years, the public concern about antibiotic-resistant microorganisms stimulated research studies on new and novel environmentally-friendly antimicrobial agents. Environmentally friendly novel antimicrobial materials can be achieved from several sources of biological material (such as animal-originated side products, plant extracts and essential oils) or synthesized organic/inorganic compounds [71-73]. Since their high surface area to volume ratio and unmatched physical and chemical characteristics, nanostructured inorganic metal compounds have been previously shown to retain potent antimicrobial effects at even very low concentrations used without or with the minimal effect on human cells [71-75]. The chemical composition and antimicrobial activities of plant extracts, essential oils, and

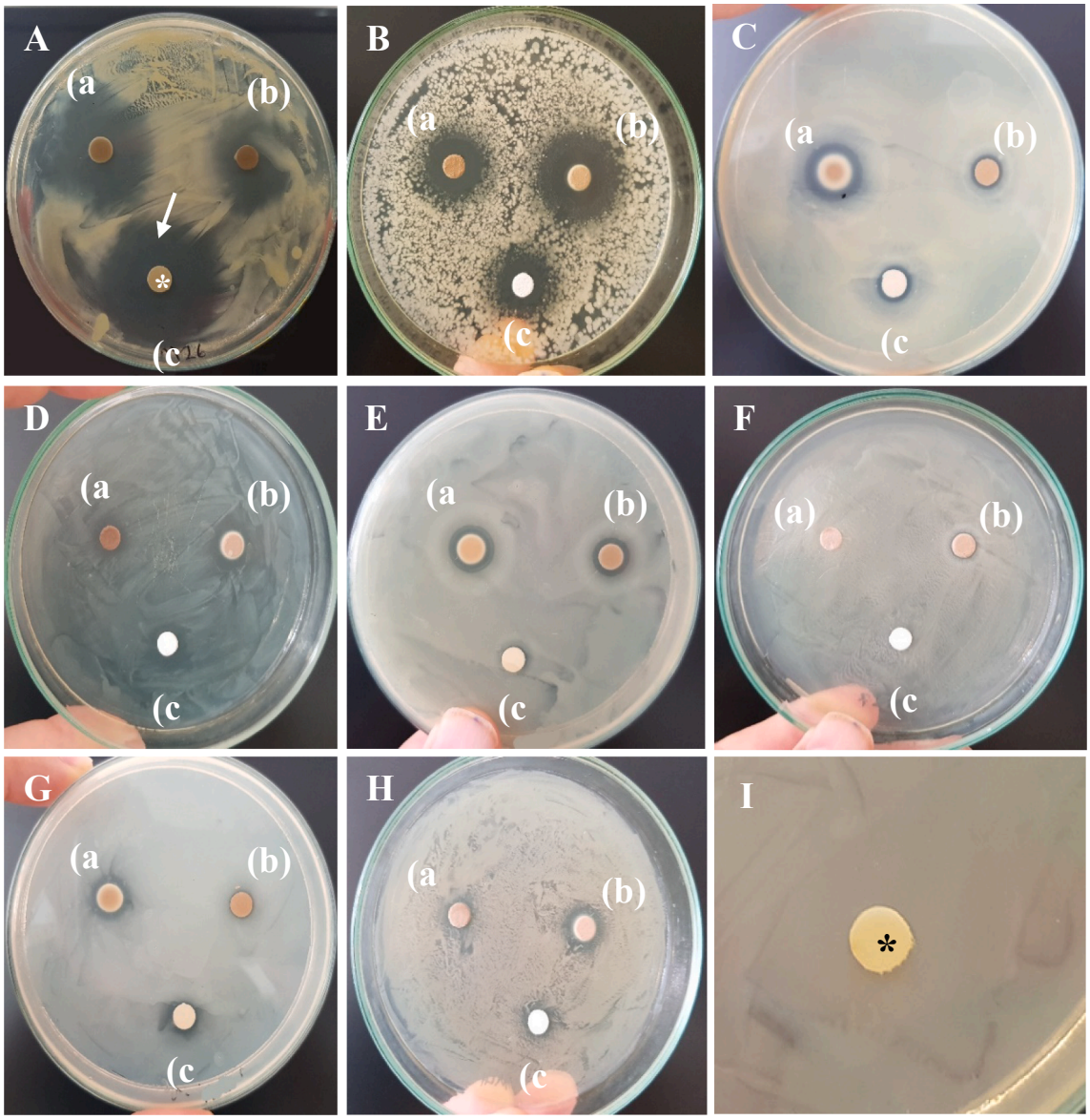

Fig. 14. Antibacterial activities of green synthesized ZnO-NPs using *T. syriacus* extract against different bacterial disease agents *C. michiganensis* subsp. *michiganensis* (**A**), *Bacillus subtilis* subsp. *subtilis* (**B**), *Pseudomonas cichorii* (**C**), *Pseudomonas syringae* pv. *phaseolicola* (**D**), *Pectobacterium carotovorum* subsp. *carotovorum* (**E**), *Pseudomonas corrugata* (**F**), *Pseudomonas syringae* pv. *syringae* (**G**); *Xanthomonas axonopodis* pv. *juglandis* (**H**). Note clear zone of inhibition (arrow) around the filter disc (*) containing 10 μL of the 5.0 % ZnO-NPs (**a**), 2.5 % ZnO-NPs (**b**) and bare ZnO nanoparticles (**c**), in each petri plates. Note absence of inhibition zones around filter disc (*) containing 10 μL of the pure DMSO (**I**).

Table 3
Determination of antibacterial activities caused by green synthesized ZnO-NPs against different species of bacterial disease agents by using agar disc diffusion assay.

Treatments	Zone of inhibition (mm)[a] against bacterial disease agents							
	*Cmm*A12	*Bss*A19	*Pc*Sa2	*Psp*E22	*Pcc*Sy17	*Pcor*Sa27	*Pss*E8	*Xaj*E5
Bare ZnO	28.67fB	14.67eB	9.00cB	11.00 dB	6.33abB	6.00aA	7.67bcB	8.00cB
2.5 % *T. syriacus*	30.33eB	15.67 dB	12.67cC	11.33cB	8.67bC	6.00aA	9.33bC	8.67bB
5.0 % *T. syriacus*	35.00eC	20.33dC	17.00cD	19.33cdC	12.33bD	7.00aA	14.00bD	13.33bC
Negative Control	0.0A	0.0A	0.0A	0.0A	0.0A	0.0A	0.0A	0.0A

Cmm: C. michiganensis subsp. michiganensis; Pc: Pseudomonas cichorii; Psp: P. syringae pv. phaseolicola; Pcc: P. caratovorum subsp. carotovorum; Pcor: Pseudomonas corrugata; Pss: Pseudomonas syringae pv. syringae; Xaj; Xanthomonas axonopodis pv. juglandis; Bss: Bacillus subtilis subsp. Subtilis.

[a] Inhibition zones (mm) measured 24 days after inoculation. Inhibition zone includes diameter of disc (5 mm). ± indicates standard error of means. Means in the rows and columns followed by different small and capital letters are significantly different according to Duncan's Multiple Range Test ($P \leq 0.05$).

their major compounds from different medicinal plant species were previously evaluated against the wide range of human, plant, and food spoiling bacterial, fungal, and viral microorganisms [76]. Because of several advantages, ZnO-NPs that were fortified with plant extracts, are a choice as a new novel antimicrobial substance [77].

In several studies, ZnO-NPs were described as an antimicrobial agent against a wide range of both human and food spoilage microorganisms [71,78-80]. Although antimicrobial activities of green synthesized NPs

have been rarely addressed against very few plant pathogenic fungal and bacterial disease agents [34-36,81], the antibacterial activities of green synthesized NPs using *T. syriacus* aqueous leaf extract against plant pathogenic bacterial disease agents were not studied previously.

Essential oils of plants belonging Lamiaceae family were reported to be rich in phenolic compounds, which are believed to be responsible for the marked antimicrobial activity [33,38,82] reported chemical compositions and antibacterial activities of the essential oil of *T. syriacus*, which contains high percentage of carvacrol and thymol as major components. The antimicrobial activities of the essential oils and phenolic compounds could be attributed to their hydrophobic nature that allows these compounds to penetrate microbial cells and cause alterations in their structure and functionality, as reported [82-84]. The involvement of essential oil components may disrupt the bacterium's cell membrane and change its permeability as reported by [83]. Essential oils and their major components of oregano, thyme and thymus have been reported to induce rapid cell lysis of certain fungal and bacterial disease agents [38,84,85].

Although the process underlying the antibacterial effect of ZnO-NPs was not studied in the current study, previous studies have reported that membrane deterioration owing to the accumulation of ZnO-NPs therein and internalization of nanoparticles followed by the release of antimicrobial Zn^{+2} ions was the primary mode of action of the antibacterial effect of green synthesized ZnO-NPs [71,86,87]. The stimulation of oxidative stress because of the formation of hydrogen peroxide (H_2O_2), a strong oxidizing reactive oxygen species which is harmful to bacterial cells, was also reported as another mode of action of antimicrobial activities of ZnO-NPs [88,89]. The induction of H_2O_2 by ZnO-NPs at the reaction sites may cause membrane leakage of the cytosol of the bacterial cell and the inactivation of respiratory chain dehydrogenase, which was possibly responsible for the enhanced antibacterial efficiencies of nanostructured materials. Antibacterial activities of green synthesized ZnO-NPs were also demonstrated by morphocellular studies by using Scanning (SEM) and Transmission Electron Microscopes (TEM). Following the treatment of bacterial cells with ZnO-NP, nanoparticles caused considerable morphological changes in the cell membrane. Following accumulation in the cytoplasm, ZnO-NPs interact with biomolecules, eventually leading to cell death [90].

4. Conclusion

In this study, ZnO-NPs were successfully synthesized by using different concentrations of *T. syriacus* plant extract by the SILAR method. The ZnO-NPs have hexagonal structures (wurtzite phases) and the crystallite size changes from 17.19 nm to 14.51 nm. The SEM and AFM pictures revealed the homogenous distribution of well-defined spherical-like morphology ZnO-NPs depending on the concentration of *T. syriacus*. EDX results verified the existence of Zn and O components in the synthesized ZnO-NPs. The absorption peaks at ~ 853 cm^{-1}, 728 cm^{-1}, and ~ 560 cm^{-1} in the FTIR spectrum are dedicated to stretching modes of the Zn-O bond. The energy bandgap calculated from Tauc's relation with various *T. syriacus* concentrations was found to be in the range 3.17–3.28 eV. Cole-Cole plots indicate the presence of a single semicircle for all the ZnO-NPs and their radius defined with % *T. syriacus* addictives, which affect grain boundary resistance. This study also demonstrated that the green synthesis of ZnO-NPs with the use of *T. syriacus* aqueous leaf extract is a promising choice against plant pathogenic bacterial disease agents.

CRediT authorship contribution statement

B. Şahin: Investigation, Methodology, Formal analysis, Data curation, Writing – review & editing, Supervision. **R. Aydin:** Investigation, Data curation, Writing – review & editing. **S. Soylu:** Methodology, Data curation, Writing – review & editing, Supervision. **M. Türkmen:** Investigation, Methodology, Data curation. **M. Kara:** Investigation, Methodology, Data curation. **A. Akkaya:** Data curation, Writing – review & editing. **H. Çetin:** Data curation, Writing – review & editing. **E. Ayyıldız:** Data curation, Supervision.

Declaration of Competing Interest

The authors declare that they have no known competing financial interests or personal relationships that could have appeared to influence the work reported in this paper.

Acknowledgement

None.

References

[1] B. Sahin, T. Kaya, Enhanced hydration detection properties of nanostructured CuO films by annealing, Microelectronical Eng. 164 (2016) 88–92.
[2] W.A. Khaleel, S.A. Sadeq, I.A.M. Alani, M.H.M. Ahmed, Magnesium oxide (MgO) thin film as saturable absorber for passively mode locked erbium-doped fiber laser, Opt. Laser Technol. 115 (2019) 331–336.
[3] Z.N. Kayani, S. Rahim, R. Sagheer, S. Riaz, S. Naseem, Assessment of antibacterial and optical features of sol-gel dip coated La doped TiO_2 thin films, Mater. Chem. Phys. 250 (2020), 123217.
[4] K.R. Ahammed, M.d. Ashaduzzaman, S.C. Paul, M.R. Nath, S. Bhowmik, O. Saha, M.M. Rahaman, S. Bhowmik, T.D. Aka, Microwave assisted synthesis of zinc oxide (ZnO) nanoparticles in a noble approach: utilization for antibacterial and photocatalytic activity, SN Appl. Sci. 2 (2020) 955.
[5] G. Kasi, K. Viswanathan, J. Seo, Effect of annealing temperature on the morphology and antibacteria activity of Mg-doped zinc oxide nanorods, Ceram. Int. 45 (2019) 3230–3238.
[6] I. Shtepliuk, V. Khranovskyy, D. Gogova, M. Danilson, M. Krunks, I.G. Ivanov, R. Yakimov, Excitonic emission in heavily Ga-doped zinc oxide films grown on GaN, J. Lumin. 223 (2020), 117265.
[7] B.N. Patil, T.C. Taranath, Limonia acidissima L. leaf mediated synthesis of silver and zinc oxide nanoparticles and their antibacterial activities, Microb. Pathog. 115 (2018) 227–232.
[8] A. Manikandan, E. Manikandan, B. Meenatchi, S. Vadivel, S.K. Jaganathan, R. Ladchumananandasivam, M. Henini, M. Maaza, J.S. Aanand, Rare earth element (REE) lanthanum doped zinc oxide (La: ZnO) nanomaterials: Synthesis structural optical and antibacterial studies, J. Alloy. Compd. 723 (2017) 1155–1161.
[9] V. Galstyan, E. Comini, C. Baratto, G. Faglia, G. Sberveglieri, Nanostructured ZnO chemical gas sensors, Ceram. Int. 41 (10) (2015) 14239–14244.
[10] A. Sosna-Głębska, M. Sibiński, N. Szczecińska, A. Apostoluk, UV–Visible silicon detectors with zinc oxide nanoparticles acting as wavelength shifters, Mater. Today:. Proc. 20 (2020) 25–29.
[11] A.M. Pillai, V.S. Sivasankarapillai, A. Rahdar, J. Joseph, F. Sadeghfar, K. Rajesh, G. Z. Kyzas, Green synthesis and characterization of zinc oxide nanoparticles with antibacterial and antifungal activity, J. Mol. Struct. 1211 (2020), 128107.
[12] N. Matinise, X.G. Fuku, K. Kaviyarasu, N. Mayedwa, M. Maaza, ZnO nanoparticles via Moringa oleifera green synthesis: Physical properties & mechanism of formation, Appl. Surf. Sci. 406 (2017) 339–347.
[13] G. Sharmila, M. Thirumarimurugan, C. Muthukumaran, Green synthesis of ZnO nanoparticles using *Tecoma castanifolia* leaf extract: Characterization and evaluation of its antioxidant, bactericidal and anticancer activities, Microchem. J. 145 (2019) 578–587.
[14] X. Huang, X. Zheng, Z. Xu, C. Yi, ZnO-based nanocarriers for drug delivery application: From passive to smart strategies, Int. J. Pharm. 534 (2017) 190–194.
[15] A.K. Ambedkar, M. Singh, V. Kumar, V. Kumar, B.P. Singh, A. Kumar, Y.K. Gautam, Structural, optical and thermoelectric properties of Al-doped ZnO thin films prepared by spray pyrolysis, Surf. Interfaces 19 (2020), 100504.
[16] Irshad Ahmad, Muhammad Shoaib Akhtar, Ejaz Ahmed, Mukhtar Ahmad, Facile synthesis of Pr-doped ZnO photocatalyst using sol–gel method and its visible light photocatalytic activity, J. Mater. Sci.: Mater. Electron. 31 (2) (2020) 1084–1093.
[17] Sayed M. Saleh, ZnO nanospheres based simple hydrothermal route for photocatalytic degradation of azo dye, Spectrochim. Acta Part A Mol. Biomol. Spectrosc. 211 (2019) 141–147.
[18] Abdelkader Nebatti, Christian Pflitsch, Burak Atakan, Unusual application of aluminium-doped ZnO thin film developed by metalorganic chemical vapour deposition for surface temperature sensor, Thin Solid Films 636 (2017) 532–536.
[19] V.K. Ashith, Gowrish K. Rao, Sahana N. Moger, Smitha R, Smitha R, Effect of post-deposition annealing on the properties of ZnO films obtained by high temperature, micro-controller based SILAR deposition, Ceram. Int. 44 (9) (2018) 10669–10676.
[20] S.U. Offiah, S.N. Agbo, P. Sutta, M. Maaza, P.E. Ugwuoke, R.U. Osuji, F.I. Ezema, Study of the extrinsic properties of ZnO: Al grown by SILAR technique, J. Solid State Electrochem. 21 (9) (2017) 2621–2628.
[21] Vithoba L. Patil, Sharadrao A. Vanalakar, Pramod S. Patil, Jin H. Kim, Fabrication of nanostructured ZnO thin films based NO_2 gas sensor via SILAR technique, Sens. Actuators, B 239 (2017) 1185–1193.
[22] A. Tasdemir, R. Aydin, A. Akkaya, N. Akman, Y. Altınay, H. Çetin, B. Sahin, A. Uzun, E. Ayyıldız, A green approach for the preparation of nanostructured zinc

oxide: Characterization and promising antibacterial behavior, Ceram. Int. 47 (2021) 19362–19373.
[23] Khatereh Pakzad, Heshmatollah Alinezhad, Mahmoud Nasrollahzadeh, Green synthesis of Ni@Fe_3O_4 and CuO nanoparticles using *Euphorbia maculata* extract as photocatalysts for the degradation of organic pollutants under UV-irradiation, Ceram. Int. 45 (14) (2019) 17173–17182.
[24] M. Kamali, F. Samari, F. Sedaghati, Low-temperature phyto-synthesis of copper oxide nanosheets: its catalytic effect and application for colorimetric sensing, Mater. Sci. Eng., C 103 (2019), 109744.
[25] S. Sundar, G. Venkatachalam, S.J. Kwon, Biosynthesis of copper oxide (CuO) nanowires and their use for the electrochemical sensing of dopamine, Nanomaterials 8 (2018) 1–17.
[26] B.T. Sone, A. Diallo, X.G. Fuku, A. Gurib-Fakim, M. Maaza, Biosynthesized CuO nano-platelets: physical properties & enhanced thermal conductivity nanofluidics, Arabian J. Chem. 13 (2020) 160–170.
[27] Ajay K. Potbhare, Ratiram Gomaji Chaudhary, Prashant B. Chouke, Sachin Yerpude, Aniruddha Mondal, Vaishali N. Sonkusare, Alok R. Rai, Harjeet D. Juneja, Phytosynthesis of nearly monodisperse CuO nanospheres using *Phyllanthus reticulatus/Conyza bonariensis* and its antioxidant/antibacterial assays, Mater. Sci. Eng., C 99 (2019) 783–793.
[28] Saee Gharpure, Aman Akash, Balaprasad Ankamwar, A Review on antimicrobial properties of metal nanoparticles, J. Nanosci. Nanotechnol. 20 (6) (2020) 3303–3339.
[29] G.W. Sundin, L.F. Castiblanco, X. Yuan, Q. Zeng, C.-H. Yang, Bacterial disease management: challenges, experience, innovation and future prospects, Mol. Plant Pathol 17 (2016) 1506–1518.
[30] M. Mengulluoglu, S. Soylu, Antibacterial activities of essential oils from several medicinal plants against the seed-borne bacterial disease agent *Acidovorax avenae* subsp. *citrulli*, Research on, Crops 13 (2012) 641–646.
[31] B. Ranjithkumar, H.B. Ramalingam, E. Ranjith Kumar, Ch. Srinivas, G. Magesh, C. Sharmila Rahale, Nashwa M. El-Metwaly, B. Chandar Shekar, Natural fuels (Honey and Cow urine) assisted combustion synthesis of zinc oxide nanoparticles for antimicrobial activities, Ceram. Int. 47 (10) (2021) 14475–14481.
[32] A.D. Azaz, H.A. Irtem, M. Kurkcuoğlu, K.H. Baser, Composition and the *in vitro* antimicrobial activities of the essential oils of some *Thymus* species, Zeitschrift für Naturforschung C 59 (2004) 75–80.
[33] A. Al-Mariri, G. Swied, A. Oda, L. Al Hallab, Antibacterial activity of *Thymus syriacus* boiss essential oil and its components against some Syrian Gram-negative bacteria isolates, Iranian, J. Medical Sci. 38 (2013) 180–186.
[34] S. Pandey, K. Giri, R. Kumar, G. Mishra, R. Raja Rishi, Nanopesticides: opportunities in crop protection and associated environmental risks, Proceedings of the National Academy of Sciences, India Section B: Biological Sciences 88 (4) (2018) 1287-1308.
[35] M. Naseer, U. Aslam, B. Khalid, B. Chen, Green route to synthesize Zinc Oxide Nanoparticles using leaf extracts of Cassia fistula and Melia azadarach and their antibacterial potential, Sci. Rep. 10 (2020), 9055.
[36] B. Şahin, S. Soylu, M. Kara, M. Türkmen, R. Aydin, H. Çetin, Superior antibacterial activity against seed-borne plant bacterial disease agents and enhanced physical properties of novel green synthesized nanostructured ZnO using Thymbra spicata plant extract, Ceram. Int. 47 (1) (2021) 341–350.
[37] Z.C. Aktan, S. Soylu, Diyarbakır ilinde yetişen badem ağaçlarından endofit ve epifit bakteri türlerinin izolasyonu ve bitki gelişimini teşvik eden mekanizmalarının karakterizasyonu, Kahramanmaraş Sütçü İmam Üniversitesi Tarım ve Doğa Dergisi 23 (3) (2020) 641–654.
[38] I.A. Bozkurt, S. Soylu, M. Kara, E.M. Soylu, Chemical composition and antibacterial activity of essential oils isolated from medicinal plants against gall forming plant pathogenic bacterial disease agents, Kahramanmaraş Sütçü İmam Üniversitesi Tarım ve Doğa Dergisi 23 (2020) 1474–1482.
[39] Shiv Shankar, Jong-Whan Rhim, Effect of Zn salts and hydrolyzing agents on the morphology and antibacterial activity of zinc oxide nanoparticles, Environ. Chem. Lett. 17 (2) (2019) 1105–1109.
[40] S.H. Ribut, C.A.C. Abdullah, M. Mustafa, M.Z.M. Yusoff, S.N.A. Azman, Influence of pH variations on zinc oxide nanoparticles and their antibacterial activity, Mater. Res. Express 6 (2019), 025016.
[41] Ragia M. Mohsen, Samir M.M. Morsi, Mohamed M. Selim, Ahmed M. Ghoneim, Hazem M. El-Sherif, Electrical, thermal, morphological, and antibacterial studies of synthesized polyaniline/zinc oxide nanocomposites, Polym. Bull. 76 (1) (2019) 1–21.
[42] S. Mudassar Muzaffar, Samia Naeem, Saima Yaseen, Saira Riaz, Zohra N. Kayani, Shahzad Naseem, Microwave assisted tuning of optical and magnetic properties of zinc oxide nanorods—efficient antibacterial and photocatalytic agent, J. Sol-Gel Sci. Technol. 95 (1) (2020) 88–100.
[43] Mehdi Rezapour, Nasrin Talebian, Synthesis and investigation of Indium doping and surfactant on the morphological, optical and UV/Vis photocatalytic properties of ZnO nanostructure, Ceram. Int. 40 (2) (2014) 3453–3460.
[44] B. Şahin, T. Kaya, Facile preparation and characterization of nanostructured ZnO/CuO composite thin film for sweat concentration sensing applications, Mater. Sci. Semicond. Process. 121 (2021), 105428.
[45] M.Y.A. Rahman, A.A. Umar, R. Taslim, M.M. Salleh, Effect of surfactant on the physical properties of ZnO nanorods and the performance of ZnO photoelectrochemical cell, J. Exp. Nanosci. 10 (8) (2015) 599–609.
[46] Iqbal Singh, R.K. Bedi, Surfactant-assisted synthesis, characterizations, and room temperature ammonia sensing mechanism of nanocrystalline CuO, Solid State Sci. 13 (11) (2011) 2011–2018.
[47] Morteza Yadi, Ebrahim Mostafavi, Bahram Saleh, Soodabeh Davaran, Immi Aliyeva, Rovshan Khalilov, Mohammad Nikzamir, Nasrin Nikzamir, Abolfazl Akbarzadeh, Yunes Panahi, Morteza Milani, Current developments in green synthesis of metallic nanoparticles using plant extracts: a review, Artif. Cells Nanomed. Biotechnol. 46 (sup3) (2018) S336–S343.
[48] H.M. Pathan, C.D. Lokhande, Deposition of metal chalcogenide thin films by successive ionic layer adsorption and reaction (SILAR) method, Bull Mater Sci 27 (2) (2004) 85–111.
[49] T. Thilagavathi, D. Geetha, Nano ZnO structures synthesized in presence of anionic and cationic surfactant under hydrothermal process, Applied, Nanoscience 4 (2) (2014) 127–132.
[50] A.N. El-Shazly, M.M. Rashad, E.A. Abdel-Aal, I.A. Ibrahim, M.F. El-Shahat, A. E. Shalan, Nanostructured ZnO photocatalysts prepared via surfactant assisted Co-Precipitation method achieving enhanced photocatalytic activity for the degradation of methylene blue dyes, J. Environ. Chem. Eng. 4 (3) (2016) 3177–3184.
[51] A. Jayachandran, T.R. Aswathy, S. Nair Achuthsankar, Green synthesis and characterization of zinc oxide nanoparticles using Cayratia pedata leaf extract (L), Biochem. Biophys. Rep. 26 (2021) 100995.
[52] Shabnam Fakhari, Mina Jamzad, Hassan Kabiri Fard, Green synthesis of zinc oxide nanoparticles: a comparison, Green Chem. Lett. Rev. 12 (1) (2019) 19–24.
[53] C.R. Martinez, P. Joshi, J.L. Vera, J.E. Ramirez-Vick, O. Perales, S.P. Singh, Cytotoxic studies of PEG functionalized ZnO nanoparticles on MCF-7 cancer cells, in: NSTI Nanotechnol. Conf. Expo, NSTI-nanotech, 2011.
[54] N. Rao, M. Rao, Structural and optical investigation of ZnO nanopowders synthesized from zinc chloride and zinc nitrate, American, J. Mater. Sci. 5 (2015) 66–68.
[55] M. Sathya, A. Claude, P. Govindasamy, K. Sudha, A. Claude, Growth of pure and doped ZnO thin films for solar cell applications, Adv. in Appl. Sci. Res. 3 (2012) 2591–2598.
[56] G. Tümen, K. H.C. Baser, Essential oil of *Thymus syriacus* Boiss, J. Essent. Oil Res. 6 (6) (1994) 663–664.
[57] S. Kumar, M. Shandilya, S. Thakur, N. Thakur, Structural, optical and photoluminescence properties of $K_{0.5}Na_{0.5}NbO_3$ ceramics synthesized by sol–gel reaction method, J Sol-Gel Sci Technol 88 (2018) 646–653.
[58] L. Srinivasa Rao, T. Venkatappa Rao, Sd. Naheed, P. Venkateswara Rao, Structural and optical properties of zinc magnesium oxide nanoparticles synthesized by chemical co-precipitation, Mater. Chem. Phys. 203 (2018) 133–140.
[59] Guru Nisha Narayanan, Karthigeyan Annamalai, Role of hexamethylenetetramine concentration on structural, morphological, optical and electrical properties of hydrothermally grown zinc oxide nanorods, J. Mater. Sci.: Mater. Electron. 27 (11) (2016) 12209–12215.
[60] Bünyamin Şahin, Raşit Aydın, Hidayet Çetin, Variation of the key morphological, structural, optical and electrical properties of SILAR CdO with alkaline earth Ca^{2+} ions doping, Ceram. Int. 45 (14) (2019) 16748–16758.
[61] H. Ben Wannes, R.Benabderrahmane Zaghouani, R. Ouertani, A. Araújo, M. J. Mendes, H. Aguas, E. Fortunato, R. Martins, W. Dimassi, Study of the stabilizer influence on the structural and optical properties of sol-gel spin coated zinc oxide films, Mater. Sci. Semicond. Process. 74 (2018) 80–87.
[62] A. Akkaya, B. Şahin, R. Aydın, H. Çetin, E. Ayyıldız, Solution-processed nanostructured ZnO/CuO composite films and improvement its physical properties by lustrous transition metal silver doping, J. Mater. Sci.: Mater. Electron. 31 (17) (2020) 14400–14410.
[63] Vinod Kumar, Neetu Singh, R.M. Mehra, Avinashi Kapoor, L.P. Purohit, H.C. Swart, Role of film thickness on the properties of ZnO thin films grown by sol-gel method, Thin Solid Films 539 (2013) 161–165.
[64] R. Mariappan, V. Ponnuswamy, P. Suresh, N. Ashok, P. Jayamurugan, A. Chandra Bose, Influence of film thickness on the properties of sprayed ZnO thin films for gas sensor applications, Superlattices Microstruct. 71 (2014) 238–249.
[65] Mohd Arshad, Arham S. Ahmed, A.H. Ameer Azam, Naqvi, Exploring the dielectric behavior of Co doped ZnO nanoparticles synthesized by wet chemical route using impedance spectroscopy, J. Alloy. Compd. 577 (2013) 469–474.
[66] A. Azam, A.S. Ahmed, M.S. Ansari, M.M. Shafeeq, A.H. Naqvi, Study of electrical properties of nickel doped SnO_2 ceramic nanoparticles, J. Alloy. Compd. 506 (2010) 237–242.
[67] S. Thakur, M. Shandilya, M.P.F. Graça, M.A. Valente, To study the effect of low temperature crystal growth on the structural and ferroelectric properties of lead-free BCT-BZT ceramic, Ferroelectr. Lett. Sect. 47 (2020) 76–89.
[68] S.A. Ansari, A. Nisar, B. Fatma, W. Khan, A.H. Naqvi, Investigation on structural, optical and dielectric properties of Co doped ZnO nanoparticles synthesized by gel-combustion route, Mater. Sci. Eng., B 177 (2012) 428–435.
[69] R. Selvamani, G. Singh, V.S. Tiwari, Grain size effect on impedance and modulus properties of (Na0.5Bi0.5TiO3) (1–x) (BaZrO3) x ceramics, Mater. Res. Express 3 (2016), 056301.
[70] Mamta Shandilya, Ritesh Verma, Impedance modulated dielectric and magnetic properties of BCT-NF multiferroic composite, J. Magn. Magn. Mater. 527 (2021) 167782, https://doi.org/10.1016/j.jmmm.2021.167782.
[71] Azhwar Raghunath, Ekambaram Perumal, Metal oxide nanoparticles as antimicrobial agents: a promise for the future, Int. J. Antimicrob. Agents 49 (2) (2017) 137–152.
[72] R. Swati, A. Verma, M. Chauhan, X. Shandilya, R. Li, S. Kumar, Kulshrestha, Antimicrobial potential of Ag-doped ZnO nanostructure synthesized by the green method using Moringa oleifera extract, Journal of Environmental, Chem. Eng. 8 (2020), 103730.
[73] S. Thakur, M. Shandilya, G. Guleria, Appraisement of antimicrobial zinc oxide nanoparticles through Cannabis Jatropha curcasa Alovera and Tinosporacordifolia leaves by green synthesis process, J. Environ. Chem. Eng. 9 (2021), 104882.

[74] A. Husen, Gold nanoparticles from plant system: Synthesis, characterization and their application, In: Nanoscience and Plant–Soil Systems Vol.–48 (Eds. Ghorbanpourn M, Manika K, Varma A) Springer International Publishing AG, Gewerbestrasse 11 (2017), 6330 Cham, Switzerland, pp.455–479.
[75] Q. Chaudhry, M. Scotter, J. Blackburn, B. Ross, A. Boxall, L. Castle, R. Aitken, R. Watkins, Applications and implications of nanotechnologies for the food sector, Food Additives & Contaminants: Part A 25 (2008) 241–258.
[76] F. Bakkali, S. Averbeck, D. Averbeck, M. Idaomar, Biological effects of essential oils-A review, Food Chem. Toxicol. 46 (2) (2008) 446–475.
[77] K. Elumalai, S. Velmurugan, Green synthesis, characterization and antimicrobial activities of zinc oxide nanoparticles from the leaf extract of *Azadirachta indica* (L), Appl. Surf. Sci. 345 (2015) 329–336.
[78] Krishna R Raghupathi, Ranjit T Koodali, Adhar C Manna, Size-dependent bacterial growth inhibition and mechanism of antibacterial activity of zinc oxide nanoparticles, Langmuir 27 (7) (2011) 4020–4028.
[79] Ling Chuo Ann, Shahrom Mahmud, Siti Khadijah Mohd Bakhori, Amna Sirelkhatim, Dasmawati Mohamad, Habsah Hasan, Azman Seeni, Rosliza Abdul Rahman, Antibacterial responses of zinc oxide structures against *Staphylococcus aureus*, *Pseudomonas aeruginosa* and *Streptococcus pyogenes*, Ceram. Int. 40 (2) (2014) 2993–3001.
[80] Lesley L. Duffy, Megan J. Osmond-McLeod, Jonathan Judy, Thea King, Investigation into the antibacterial activity of silver, zinc oxide and copper oxide nanoparticles against poultry-relevant isolates of *Salmonella* and *Campylobacter*, Food Control 92 (2018) 293–300.
[81] Ileana Vera-Reyes, Itandehui Juanita Erendira Esparza-Arredondo, Ricardo Hugo Lira-Saldivar, Carlos Alejandro Granados-Echegoyen, Rocío Alvarez-Roman, Alfonso Vásquez-López, Gladys De los Santos-Villarreal, Enrique Díaz-Barriga Castro, *In vitro* antimicrobial effect of metallic nanoparticles on phytopathogenic strains of crop plants, J. Phytopathol. 167 (7-8) (2019) 461–469.
[82] Karina Kachur, Zacharias Suntres, The antibacterial properties of phenolic isomers, carvacrol and thymol, Crit. Rev. Food Sci. Nutr. 60 (18) (2020) 3042–3053.
[83] G.C. Lucas, E. Alves, R.B. Pereira, F.J. Perina, R.M. de Souza, Antibacterial activity of essential oils on *Xanthomonas vesicatoria* and control of bacterial spot in tomato, Pesquisa Agropecuária Brasileira 47 (2012) 351–359.
[84] R.S. da Silva, M.M.G. de Oliveira, J.O. de Melo, A.F. Blank, C.B. Correa, R. Scher, R. P.M. Fernandes, Antimicrobial activity of *Lippia gracilis* essential oils on the plant pathogen *Xanthomonas campestris* pv. *campestris* and their effect on membrane integrity, Pestic. Biochem. Physiol. 160 (2019) 40–48.
[85] Q.C. Liu, K. Qiao, S.A. Zhang, Potential of a small molecule carvacrol in management of vegetable diseases, Molecules 24 (2019) 1932.
[86] A. Sirelkhatim, S. Mahmud, A. Seeni, N.H.M. Kaus, L.C. Ann, S.K.M. Bakhori, D. Mohamad, Review on zinc oxide nanoparticles: Antibacterial activity and toxicity mechanism, Nano-Micro Letters 7 (2015) 219–242.
[87] Roberta Brayner, Roselyne Ferrari-Iliou, Nicolas Brivois, Shakib Djediat, Marc F. Benedetti, Fernand Fiévet, Toxicological impact studies based on *Escherichia coli* bacteria in ultrafine ZnO nanoparticles colloidal medium, Nano Lett. 6 (4) (2006) 866–870.
[88] N. Jones, B. Ray, K.T. Ranjit, A.C. Manna, Antibacterial activity of ZnO nanoparticle suspensions on a broad spectrum of microorganisms, FEMS Microbiol. Lett. 279 (1) (2008) 71–76.
[89] Qiong Liu, Ju Li, Xin Zhong, Zan Dai, Zhong Lu, Hao Yang, Rong Chen, Enhanced antibacterial activity and mechanism studies of Ag/Bi_2O_3 nanocomposites, Adv. Powder Technol. 29 (9) (2018) 2082–2090.
[90] Khwaja Salahuddin Siddiqi, Aziz ur Rahman, Tajuddin, Azamal Husen, Properties of zinc oxide nanoparticles and their activity against microbes, Nanoscale Res. Lett. 13 (1) (2018), https://doi.org/10.1186/s11671-018-2532-3.